SPECIAL FEATURE

Subdiffusive and superdiffusive transport in plane steady viscous flows

Michael A. Zaks[a,1] and Alexander Nepomnyashchy[b,1,2]

[a]Institute of Physics, Humboldt University of Berlin, 12489 Berlin, Germany; and [b]Department of Mathematics, Technion–Israel Institute of Technology, Haifa 32000, Israel

Edited by Snezhana I. Abarzhi, The University of Western Australia, Crawley, WA, Australia and accepted by Editorial Board Member David A. Weitz February 17, 2018 (received for review September 30, 2017)

Deterministic transport of passive tracers in steady laminar plane flows of incompressible viscous fluids through lattices of solid bodies or arrays of steady vortices can be anomalous. Motion along regular patterns of streamlines is often aperiodic: Repeated slow passages near stagnation points and/or solid surfaces serve for eventual decorrelation. Singularities of passage times near the obstacles, dictated by the boundary conditions, affect the character of transport anomalies: Flows past arrays of vortices are subdiffusive whereas tracers advected through lattices of solid obstacles can feature superdiffusion. We calculate the transport characteristics with the help of the simple and computationally efficient model: the special flow.

anomalous transport | laminar flows | special flow

Transport of passive tracers by flow patterns on large spatial and temporal scales is commonly quantified in terms of the effective diffusion tensor,

$$D_{ij} = \lim_{t\to\infty} \frac{1}{2t}\langle (x_i(t) - \langle x_i\rangle)(x_j(t) - \langle x_j\rangle)\rangle,\ i,j = 1,2,3, \quad [1]$$

where angular brackets denote averaging over the initial tracer position. For a wide class of flows including certain steady (1, 2) and random (3) ones as well as flows with the Lagrangian chaos (4, 5), the limit is finite and distinct from zero, and hence the large-scale dispersion is normal: The mean-squared displacement (MSD) $\langle |x_i(t) - \langle x_i\rangle|^2\rangle$ grows linearly with t.

However, the turbulent mixing (6), extensively studied in various physical contexts and on different scales (7, 8), often features unusual scaling laws for energy, momentum, and particle density transfer (9, 10). Specifically, the dependence of the tracer MSD on time can be nonlinear, invalidating the effective diffusion approach. Such anomalous transport happens, e.g., when the Lagrangian phase space has a complex structure with islands and chaotic regions (11) or in a random velocity field with slowly decaying velocity correlations (12).

Here we discuss another mechanism of anomalous transport, present even in certain laminar flows. In the simpler context of time-independent spatially periodic flow patterns (i.e., in the absence of Lagrangian chaos), persistent anomalous growth of dispersion in the comoving reference frame was reported in refs. 13–15. For this phenomenon to occur, the tracers should repeatedly visit the vicinities of stagnation points or of solid obstacles where their velocity becomes arbitrarily small. In such situations, the tracer motion features unusual spectral properties: Neither discrete nor absolutely continuous with respect to Lebesgue measure, the Fourier spectra of Lagrangian observables are supported by fractal sets. Interrelation between the spectral characteristics and the transport properties results in unconventional evolution of ensembles of tracers, carried by such flows: Despite the absence of both chaos and spatial disorder, a certain slow mixing takes place. An example of this effect is shown in Fig. 1, where an ensemble of tracers is transported by the steady viscous Stokes flow across the doubly periodic array of circular solid obstacles; repeated passages of particles arbitrarily close to the obstacle borders are enforced by the imposed irrational mean inclination of the flow. After a certain time, particles from the initially compact cloud can be found virtually everywhere in the domain.

Here we investigate transport anomalies caused in steady plane flows by singularities of the passage time. We start from description of exemplary steady flow patterns with stagnation points and stagnation zones that arise in incompressible fluids under the action of spatially periodic time-independent forces, as well as in viscous flows past solid obstacles. We quantify the logarithmic and power-law–like singularities in the distributions of passage times for tracers carried along the streamlines of such flows. We assume the sufficiently low density of particles, so that their hydrodynamic interaction can be disregarded. The main modeling tool is the special flow construction (16, 17), explained below. Simple geometry of the flow patterns allows us to replace direct solving of the partial differential equations of fluid mechanics by iterations of the special flow, based on circle maps with irrational rotation numbers. (In physical terms, rotation number for a doubly periodic flow is the tangent of the mean inclination of the streamline to the lattice axis.) Extensive numerical studies demonstrate that monotonic (power-law or logarithmic) temporal dependences of dispersion, common for all rotation numbers, are "decorated" by nonmonotonic patterns, dictated by the continued fraction representation of the rotation number. Within the formalism of the special flows, the growth rate of the mean-squared deviation can be evaluated explicitly, yielding theoretical predictions that match well the numerically obtained estimates of this growth rate. Furthermore, due to presence of singularities in the distributions of passage times, the transport is not merely anomalous, but also multifractal.

Significance

Anomalous transport is usually regarded as a manifestation of a spatiotemporal disorder. We predict a persistent anomalous dispersion of tracers in time-independent spatially periodic viscous flows, in the absence of either a Lagrangian chaos or a Brownian motion. The origin of transport anomalies is the slowdown near stagnation points and solid surfaces, responsible for singularities of the particle passage time. Remarkably, both subdiffusive and superdiffusive dispersion of tracers can be achieved by an appropriate choice of the flow geometry.

Author contributions: M.A.Z. and A.N. designed research; M.A.Z. and A.N. performed research; A.N. contributed new reagents/analytic tools; and M.A.Z. and A.N. wrote the paper.

The authors declare no conflict of interest.

This article is a PNAS Direct Submission. S.I.A. is a guest editor invited by the Editorial Board.

[1]M.A.Z. and A.N. contributed equally to this work.

[2]To whom correspondence should be addressed. Email: nepom@math.technion.ac.il.

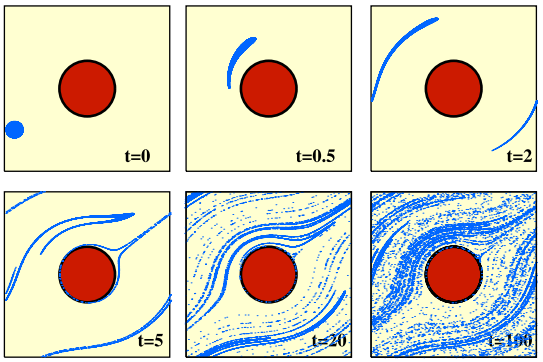

Fig. 1. Temporal evolution of the ensemble of 10^4 passive tracers transported by the steady Stokes flow through the doubly periodic array of circular solid obstacles. Positions of the particles are projected upon one basic cell of the flow. Values of *t* indicate the time instants at which the snapshots have been made.

Patterns of Forced Flows with Stagnation Points

We restrict analysis to steady 2D flows of viscous incompressible fluids. A description in terms of the stream function $\Psi(x, y)$ turns evolution of a tracer in a steady incompressible plane flow into a case of integrable Hamiltonian dynamics with one degree of freedom. Due to 2D geometry, no chaotic streamlines exist, and both Lyapunov exponents vanish identically. Constancy of velocity in every point of the physical space renders the Eulerian observables static. In contrast, the Lagrangian observables, e.g., the characteristics of a tracer carried along the isolines of Ψ, are, in general, time dependent; episodes of relatively fast motion can alternate with epochs of slow drift.

Nontrivial transport characteristics are produced by the cumulative effect of repeated passages of tracers through the regions of fast and slow motion. Seeking for a flow pattern that guarantees infinitely many returns to stagnation regions, we turn to forced flows on the 2-torus with irrational rotation number, requiring also that the vector field on the torus vanishes in certain points or along certain curves. In terms of conventional fluid mechanics, this is a flow on a square with periodic boundary conditions and nonzero mean components. Irrational rotation number ensures that the tracers repeatedly visit the stagnation region(s).

The forced flow of the incompressible fluid with density ρ and kinematic viscosity ν on the square $(0 \le x \le 2\pi,\ 0 \le y \le 2\pi)$ obeys the Navier–Stokes equation

$$\frac{\partial}{\partial t}\vec{v} + (\vec{v}\cdot\nabla)\vec{v} = -\frac{\nabla P}{\rho} + \nu\nabla^2\vec{v} + \vec{F}, \quad \nabla\cdot\vec{v} = 0, \qquad [2]$$

where $\vec{v} = (v_x, v_y)$ and P denote, respectively, the velocity and the pressure fields. The boundary conditions are periodic:

$$\vec{v}(x, y) = \vec{v}(x + 2\pi, y) = \vec{v}(x, y + 2\pi). \qquad [3]$$

Further, we impose along both coordinates the fixed nonzero mean flow across the square domain, parameterizing it by the respective flow rates α and β:

$$\int_0^{2\pi} v_x\, dy\Big|_{x=0,2\pi} = 2\pi\alpha, \quad \int_0^{2\pi} v_y\, dx\Big|_{y=0,2\pi} = 2\pi\beta. \qquad [4]$$

The forcing term $\vec{F}$ in Eq. **2** is time independent and spatially periodic; in experiments, such forces can be created in thin layers of conducting fluids by positioning at the bottom regular arrays of electrodes (18). The shape of the arising flow pattern depends on the geometry of $\vec{F}(x, y)$. It is convenient to parameterize the force by its amplitude f; a simple example is delivered, e.g., by

$$\vec{F} = (f\sin y, f\sin x, 0). \qquad [5]$$

Without forcing $(f = 0)$ the velocity field $v_x = \alpha,\ v_y = \beta$ corresponds to the linear flow on the 2-torus with straight streamlines, the same velocity value in every point, and the rotation number α/β. If the ratio α/β is rational, all streamlines are eventually closed. Below we focus on the generic case, irrational values of α/β; there, every streamline is dense on the torus, and a passive tracer carried by the flow repeatedly passes arbitrarily close to any given position. At $f = 0$ transport is the trivial translation: An ensemble of tracers, carried away from its original location, preserves its size and shape.

Introduction of weak force deforms the streamlines (Fig. 2*A*) and makes the velocity field nonuniform. However, at sufficiently small $|f|$ the qualitative picture persists: Local variations of velocity result in weak oscillations of the distance between the neighboring tracers, but on average the ensemble does not spread.

The steady solution of the Navier–Stokes equation yields time-independent components of the velocity field; in the case of the force Eq. **5**, this is

$$v_x = \alpha - \frac{f\,\cos(y-\phi_2)}{\sqrt{\beta^2+\nu^2}},\ \ v_y = \beta - \frac{f\,\cos(x-\phi_1)}{\sqrt{\alpha^2+\nu^2}} \qquad [6]$$

$$\text{with } \phi_1 = \arctan(\nu/\alpha),\ \ \phi_2 = \arctan(\nu/\beta).$$

At sufficiently small values of $|f|$ both v_x and v_y preserve their signs in the whole square domain. The picture changes when the forcing amplitude reaches the critical value $|f_{cr}|$: Cusp points, in which both velocity components vanish, appear upon certain streamlines (Fig. 2*B*). When $|f|$ is increased beyond f_{cr}, each cusp splits into a pair of stagnation points: the saddle and the elliptic

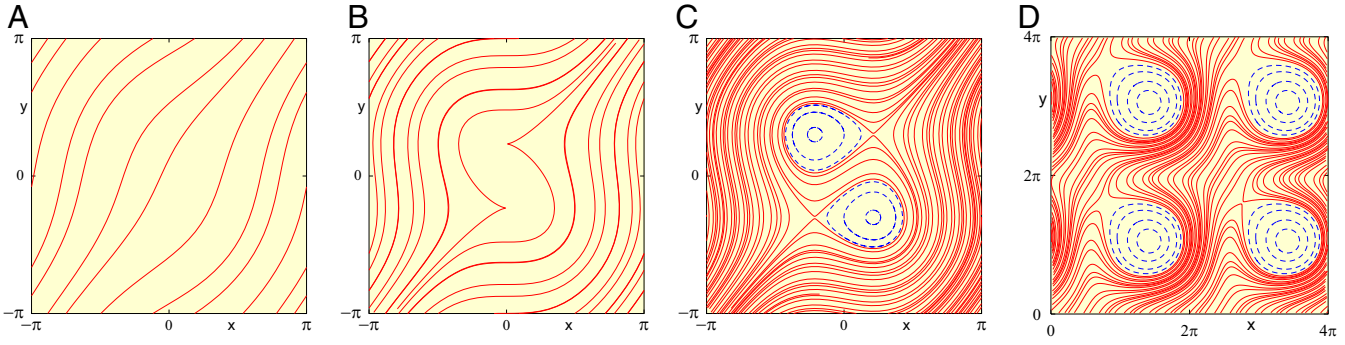

Fig. 2. (*A–D*) Patterns of streamlines on a doubly periodic domain (*A*) without singularities, $|f| < f_{cr}$; (*B*) with cusps on streamlines, $|f| = f_{cr}$; (*C*) with counterrotating vortices, $|f| > f_{cr}$; and (*D*) with corotating vortices, $|f| > f_{cr}$ (four elementary cells are shown).

point. As a consequence, vortices (eddies) appear on the torus. Each vortex, filled by nested closed streamlines, is located around one of the elliptic points and is encircled by the separatrix of one of the saddles. The forcing term from Eq. **5** generates two counterrotating vortices (Fig. 2*C*); other, more elaborate, forcing patterns can produce corotating vortices as well (Fig. 2*D* with the velocity components $v_x = \alpha + \sin y - \sin x \sin y$, $v_y = \beta x - \cos x - \cos x \cos y$). For $|f| > f_{cr}$ the phase space of the system is mixed, with simple periodic motions inside the vortices, and the global component is populated by aperiodic motions with rotation number α/β. Each trajectory outside the vortices is dense in the global component, and hence a tracer repeatedly traverses the vicinities of the saddles, whereby its velocity becomes arbitrarily small.

Whenever two initially close tracers enter the region near the saddle point, the particle with a streamline closer to the saddle is subjected to a stronger slowdown. Therefore, the former neighbors move apart and leave the stagnation region nonsimultaneously. The strongest decorrelation of this kind occurs when two particles tend to the saddle along opposite sides of its incoming separatrix: On passing the saddle, one tracer leaves the slow region along the "nonclosed" outgoing separatrix, whereas the other one encircles the vortex, enters the stagnation zone for the second time, and slows down again. The tracers stay attached to neighboring streamlines, but the average distance between them grows in the course of accumulating passages near the saddle points. In its turn, decorrelation is reflected in the spectral properties: The Fourier spectra of Lagrangian observables in Eq. **2** are neither discrete nor absolutely continuous but sit on the fractal sets (13). In a pattern like the one in Fig. 2*C* with symmetric counterrotating vortices, the repeated slowdowns and accelerations are in a rough balance, and the autocorrelation of a Lagrangian observable (say, of a velocity component) does not ultimately decay. In contrast, the configuration with corotating vortices from Fig. 2*D* is not balanced, and autocorrelation of the velocity features algebraic decay (13).

A still faster decay of correlations occurs in the hydrodynamically different situation, in which there is no forcing (save for the pressure gradient, necessary for the flow across the cells): motion of a viscous fluid through a regular lattice of solid obstacles. The flow pattern is sketched in Fig. 3.

Due to no-slip boundary conditions, both components of velocity vanish not in isolated stagnation points, but along the entire boundary of every obstacle. From the point of view of dynamics, boundaries turn into continua of fixed points, and the creeping motion along these continua is rather slow.

Singularities of Passage Time

For tracers advected by a spatially periodic velocity field, a reduction of dynamics in continuous time to the discrete Poincaré map looks natural; the boundaries of the square cell (e.g., any of the horizontal borders in the patterns from Figs. 2 and 3) serve as natural secants.

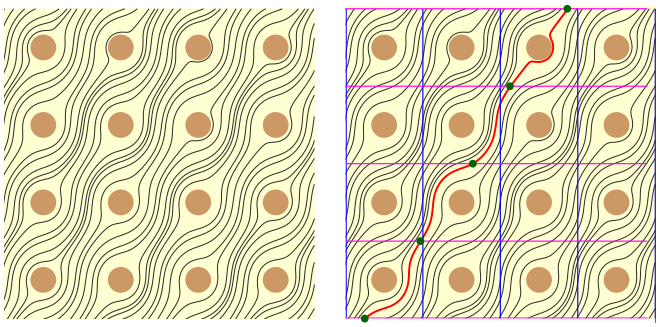

Fig. 3. (*Left*) Streamlines of the stationary Stokes flow through the regular array of solid circular cylinders (19, 20). (*Right*) Construction of the Poincaré map.

Fig. 3, *Right* shows that one-dimensional Poincaré mapping induced by the flow is equivalent to the circle shift $z \to (z + \rho) \bmod 1$ with rotation number $\rho = \alpha/\beta$. Since dynamics of such mappings are ordered, correlations do not decay along their orbits, and the power spectra are discrete. The Fourier spectra of the underlying flows, in contrast, include a (singular) continuous component whose existence is related to singularities in temporal characteristics of motion across the phase space (21). In a sense, an iteration of the mapping requires "as long" as a trajectory of the continuous flow needs for a passage from the secant onto the next secant—for a passage across the elementary cell of the flow pattern. Tracking the red streamline in Fig. 3, *Right* shows that passages close to the obstacle border alternate with passages far from it; correspondingly, the length of the time interval between the sections displays enormous fluctuations. If the stagnation points and/or obstacles are absent, this time is bounded, and the mapping dynamics mirror the dynamics of the underlying flow. The presence of vortices and obstacles, albeit leaving the mapping intact, bears a drastic influence upon the timescale: The passage (return) time $\tau_{ret}(x)$ diverges when the initial location x of a tracer approaches the streamline which exactly hits the saddle stagnation point (the incoming separatrix of the saddle) or the border of the obstacle.

Quantitatively, the cases of isolated stagnation points and solid obstacles bear different implications. We start with the flow past a structurally stable stagnation point. Straightforward linearization discloses the divergence of the passage time $\tau_{ret}(x) \sim C_{l,r} \log|x - x_0|$, where x_0 is the coordinate of intersection of the separatrix with the Poincaré secant. The prefactors C_l and C_r refer to orbits which start on the Poincaré secant, respectively, to the left and to the right of x_0. Since the streamlines on one side of x_0 encircle the vortex, the tracers on them hover near the saddle twice before returning onto the secant, while the tracers from the opposite side of x_0 go straight from the saddle to the secant. Hence, the prefactors C_l and C_r differ by the factor of 2. In the flow pattern from Fig. 2*C* with two vortices per basic cell, the passage time $\tau_{ret}(x)$ diverges in two points; due to the symmetry of the pattern, the sum of both C_l equals the sum of both C_r. In contrast, the passage time for the pattern from Fig. 2*D* has just one asymmetric ($C_r = 2C_l$) logarithmic singularity per basic cell.

Singularities of return time affect dynamical properties of the flows. In the absence of equilibria (in our case, at $f < f_{crit}$), flows on 2-tori possess a discrete spectrum and do not mix (22). Flows on 2-tori with symmetric logarithmic singularities of return time (e.g., Eq. **6** at $f > f_{crit}$) do not mix as well (23). Flows on 2-tori with asymmetric logarithmic singularities of return time (24) and the flows on 2-tori with power-law singularities of return time (25) mix.

In a generic situation of vortices encircled by separatrices of hyperbolic stagnation points, the singularities of passage time are logarithmic. Stronger singularities occur near nonhyperbolic equilibria, at the transition that transforms a flow pattern without stagnation points into the pattern with equilibria. In such critical situations, the departure along the separatrix of the newborn stagnation point is algebraic in time. In Eq. **6** at $f = f_{crit}$, as well as at the birth of corotating vortices and in similar flows without additional local degeneracies, the Hamiltonian saddle-center bifurcation takes place. Near the linearly neutral equilibrium, dynamics can be brought to the form $\ddot{z} - z^2 = 0$, and the return time diverges near the separatrix as $|x - x_0|^{-1/6}$. In the case of additional degeneracies of the vector field near the neutral stagnation point, the quadratic term (as well as some of the higher-order terms) in the equation of motion can be absent. For the appropriate normal form $\ddot{z} + z^n = 0$, $n \geq 2$, the time of passage near the neutral equilibrium diverges as $|x - x_0|^{-\kappa}$ with

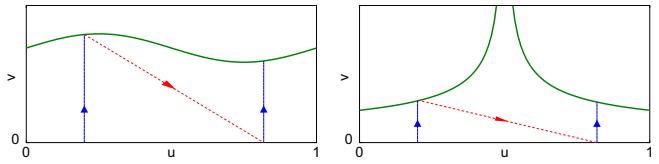

Fig. 4. Special flow over the circle map. The trajectory moves upward from the abscissa with unit velocity, until hitting the curve $T(u)$. Solid blue curve: continuous evolution. Dashed red curve: instantaneous iteration of the circle map. (*Left*) Passage time without singularities. (*Right*) Special flow with a singularity of passage time.

$$\kappa = \frac{n-1}{2n+2}. \qquad [7]$$

An example with the local mirror symmetry $n = 3$ corresponds to the "Hamiltonian pitchfork bifurcation" and $\kappa = 1/4$. For all such bifurcations of isolated equilibria in plane Hamiltonian flows, the singularities of passage time are stronger than logarithmic ones, but stay relatively weak: $\kappa < 1/2$.

Flows through arrays of solid obstacles are characterized by stronger singularities of passage time. Assuming high viscosity for the flow in Fig. 3, nonlinear terms in the equation of motion can be discarded. The resulting Stokes flow obeys, in terms of the stream function $\psi(x, y)$, the biharmonic equation $\Delta\Delta\psi = 0$, with $v_x = \partial\psi/\partial y$ and $v_y = -\partial\psi/\partial x$. In local coordinates, with the circular obstacle of radius R centered at the origin, the solution of this equation reads

$$\psi(x, y) = \frac{(\alpha y - \beta x)(x^2 + y^2 - R^2)^2}{x^2 + y^2} + h.o.t.$$

Duration of a tracer passage near the obstacle scales as $\tau_{\text{ret}} \sim |x - x_0|^{-1/2}$, where x_0, like above, marks the intersection of the Poincaré secant with the separatrix that hits the obstacle. This singularity of return time is sufficiently strong to cause the power-law decay of the autocorrelation of velocity (14).

Transport of Tracers Through Arrays of Obstacles

Power spectra of all these flow patterns, despite integrability of the underlying dynamical systems, contain the fractal component. Since transport characteristics are related to spectral properties, it is only natural to expect unconventional behavior from ensembles of tracers advected by such patterns. A compact cloud of passive tracers gets distorted and stretched with every passage near a stagnation point or a solid obstacle. As visualized in Fig. 1, integrability does not hinder mixing: After a sufficient time interval, tracers from the initially localized droplet get scattered over the whole basic cell.

The rate of the mixing process depends on the type of singularity of passage time: Slow in the presence of logarithmic singularities, mixing is much faster for the power-law–like ones. Vicinities of stagnation points/obstacles serve as a kind of trap: As the tracer ensemble is carried past the trap, some of its elements get captured and bog down, while the bulk of the ensemble moves on. As the tracers, one by one, leave the trap, new particles get into other traps farther downstream, and the ensemble becomes elongated in the stream direction. As long as no molecular diffusion is allowed, transport across the streamlines is absent. We characterize the time-dependent dispersion along the streamlines by "unwrapping" the torus onto the plane and computing the MSD in the comoving reference frame attached to the drifting center of the ensemble,

$$\xi^2(t) = \langle (x(\tau + t) - x(\tau) - \overline{v}_x t)^2 \rangle_\tau, \qquad [8]$$

where $\overline{v}_x$ is the mean velocity in the direction x and averaging is performed over the values of time τ.

According to numerical studies in refs. 13 and 14, the MSD is, on average, growing in the course of time t. Remarkably, the growth turns out to be strongly sublinear for flows with ensembles of vortices and mildly superlinear for the flow through a lattice of circular solid obstacles. This means that repeated close passages near isolated stagnation points generate subdiffusion whereas passages along the no-slip boundaries lead to superdiffusion. In this way, presence of either "hard" (solid bodies) or "soft" (vortices) obstacles in the flow pattern delivers a purely deterministic mechanism of anomalous transport.

Special Flow Construction: Flow over the Mapping

Absence of positive Lyapunov exponents results in slowness of mixing, especially in the case of relatively weak logarithmic singularities of the passage time. At nonsmall values of t, convergence of averages in Eq. **8** requires billions of passages through basic cells. This circumstance obstructs numerical estimates of the transport characteristics through direct simulations of the hydrodynamical equations, making them rather time-consuming. Below, we draw conclusions on the character of transport from simulations of a much simpler model that preserves both essential properties of dynamics: repeated passages arbitrarily close to any given point and presence of singularities of the required character in the passage times.

This model, proposed by von Neumann in ref. 16 and known in ergodic theory as the "special flow" (17), is, in a sense, a modification of the mapping that permits its iterations to possess "duration." In expressions for average characteristics of conventional mappings, all iterations share the same weight. Taking duration into account allows us to assign higher weights to long slow passages from the secant to the next secant and, respectively, lower weights to short fast passages (compare segments of the red streamline in Fig. 3, *Right*). A flow is built over the mapping in the following way: As sketched in Fig. 4, the phase space is the plane region between the abscissa, parameterized by u, and the given function $T(u)$; the latter corresponds to the passage time $\tau_{\text{ret}}(x)$. The variable u (the variable of the circle mapping) is piecewise constant. The variable v mimics the passage time; its dependence on time is piecewise continuous. Evolution starts at some abscissa point and evolves as follows: The value of u stays fixed whereas the value of the coordinate v increases with unit speed ($\dot{v} = 1$) until reaching the value $T(u)$; from there, the system instantaneously jumps into the position $\big((u + \rho) \bmod 1, 0\big)$, begins the next segment of the motion upward with unit speed, and so on.

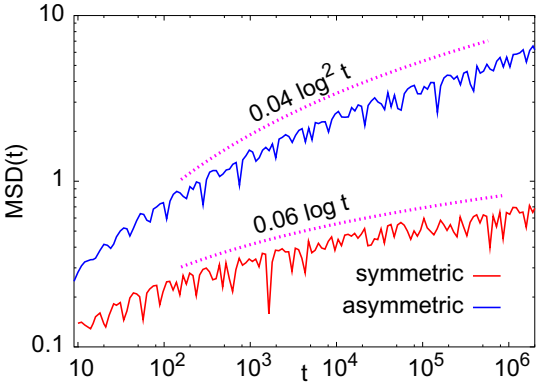

Fig. 5. Temporal evolution of MSD in special flows with logarithmic singularities of passage time. Solid lines: numerical data. Dotted curves: growth laws.

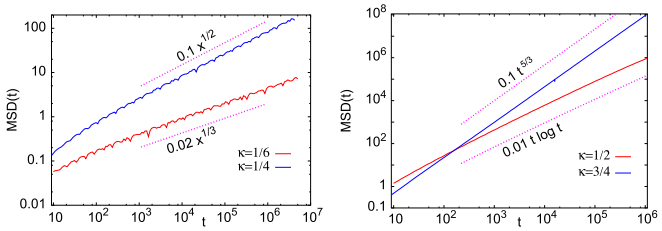

Fig. 6. Temporal growth of MSD in special flows with power-law singularities of passage time. Solid lines: numerical data. Dotted curves: growth laws. (*Left*) Subdiffusion for $T(x) \sim |x - x_0|^{-1/6}$ and $T(x) \sim |x - x_0|^{-1/4}$. (*Right*) Superdiffusion for $T(x) \sim |x - x_0|^{-1/2}$ and $T(x) \sim |x - x_0|^{-3/4}$.

The role of singularities in $T(x)$ was disclosed by von Neumann who observed that presence of a discontinuity disrupted the purely discrete spectrum by giving rise to the continuous spectral component (16). Later, special flows with different kinds of singularities were used for studies of mixing in flows on 2-tori with points of equilibrium (24, 25).

Numerical Studies

For computations of the transport characteristics, we used the special flow over the circle map $u \to (u + \rho) \bmod 1$ with golden mean rotation number $\rho = (\sqrt{5} - 1)/2$. For logarithmic divergence of passage times, the functions

$$T(u) = 1 - \log|u - 1/2|$$

$$\text{and} \quad T(u) = \begin{cases} 1 - \log|1/2 - u|, & u < 1/2 \\ 1 - \log 2 - 2\log(u - 1/2), & u > 1/2 \end{cases}$$

(respectively, symmetric and asymmetric singularities) were used. For power-law singularities, the functions $T(u) = 2|u - 1/2|^{-\kappa}$ with $0 < \kappa < 1$ were taken. As an observable we chose the "phase" ϕ of the flow, defined in a point with coordinates $u(t), v(t)$ as the ratio $v/T(u)$; ϕ varies between 0 and 1. For the lift of ϕ onto the infinite line we calculated, in accordance with Eq. **8**, the stretching MSD $\xi^2(t)$. Trajectories of the special flow until $t = 10^{11}$ were computed numerically, displaying good convergence of $\xi^2(t)$ in the range $0 < t < 10^5$.

Logarithmic Singularities of Passage Time. Fig. 5 presents temporal evolution of MSD $\xi^2(t)$ for two types of logarithmic singularities. The essential feature in both cases is remarkable nonmonotonicity of $\xi^2(t)$ that is due to the properties of dynamics on the torus with an irrational rotation number. Never closing exactly, an orbit returns from time to time arbitrarily close to any given point. Local minima of $\xi^2(t)$ correspond to the values of t at which the points on the average come especially close to their initial positions: The ensemble of particles vaguely recalls its past. Rotation number ρ rigidly orders the returns; the closest ones occur at the values of t, proportional to denominators of the best rational approximations to ρ. For the golden mean σ, the time of the nth closest return is proportional to the term F_n of the Fibonacci sequence of integers; since $\lim_{n\to\infty} F_n/F_{n+1} = \sigma$, the positions of local minima of $\xi^2(t)$ form the log-periodic sequence, well recognizable in logarithmic coordinates. In the case of a different irrational ρ, the sequence of local minima is log periodic whenever ρ is the quadratic irrational (i.e., its expansion into the continued fraction is periodic); otherwise that sequence looks disordered.

The overall (albeit nonmonotone) growth tendency in the evolution of the MSD in Fig. 5 is doubtless: The system gradually forgets its past, and the ensemble does not really contract to its initial size. Nevertheless, in the case of the symmetric singularity (the lower curve) when the passages along opposite sides of the separatrix roughly compensate each other, dispersion along the streamline grows rather slowly: After hundreds of thousands of turnovers on the torus, the mean deviation does not exceed the mere size of a basic cell. This is a very slow subdiffusion; on average, $\xi^2(t) \sim \log t$.

For the asymmetric logarithmic singularity (Fig. 5, upper curve), the growth of MSD occurs noticeably faster. Again, the general tendency is decorated by the log-periodic Fibonacci pattern. Fitting these results yields $\xi^2(t) \sim \log^2 t$.

Power-Law Singularities of Passage Time. A faster subdiffusion is observed in special flows with singularities of the return time of the kind $T(x) \sim |x - x_0|^{-\kappa}$ with $0 < \kappa < 1/2$. In the forced viscous flows the singularities of this kind correspond to critical situations: bifurcations of isolated points of equilibrium. In Fig. 6, *Left* we present numerical results for the cases $\kappa = 1/6$ (recall that this singularity occurs at the saddle-center bifurcation) and $\kappa = 1/4$ (pitchfork).

In both cases, a short initial segment with ballistic growth is followed by subdiffusion: The MSD obeys the power law with the exponent $\approx 2\kappa$. The law of average growth $\xi^2(t) \sim t^{2\kappa}$ is common for irrational values of rotation numbers ρ; individual features of ρ prescribe the sequences of closest returns and invoke oscillations of the local prefactor before $t^{2\kappa}$. Since for the golden mean rotation number the return times form the geometric progression, these oscillations are log periodic; unlike the case of logarithmic singularities, here they are masked by relatively fast growth of the MSD, but are well visible, e.g., in plots of $\xi^2(t)/t^{2\kappa}$ vs. $\log t$.

As κ approaches 1/2 from below, the subdiffusive process gets closer to normal diffusion. Recall that the singularity $T(x) \sim |x - x_0|^{-1/2}$ does not occur in flows with isolated stagnation points, but is typical for flows through arrays of solid obstacles with no-slip borders. Remarkably, exactly at $\kappa = 1/2$ the transport appears to be mildly superdiffusive: Numerical data, shown in Fig. 6, *Right*, indicate that the mean-squared elongation follows the law $\xi^2(t) \sim t \log t$. As a result, within a relatively short time the initially compact ensemble of tracers spreads in a longitudinal direction along hundreds and thousands of cells of the flow.

Increase of κ beyond 1/2 results in even faster subdiffusion. Uncommon for conventional viscous setups, singularities with $1/2 < \kappa < 1$ may be encountered in non-Newtonian flows. Simulations for special flows with values of κ from this range (e.g., the curve for $\kappa = 3/4$ in Fig. 6, *Right*) invariably indicate superdiffusion; on approaching $\kappa = 1$, the transport becomes nearly ballistic.

Theoretical Estimates

The value of the growth exponent as well as the estimate for the corresponding global prefactor can be derived explicitly via the evaluation of the dispersion of the time that a special flow with the prescribed singularity requires for carrying out $n \gg 1$ iterations of the circle map. Approximation of the map iterations

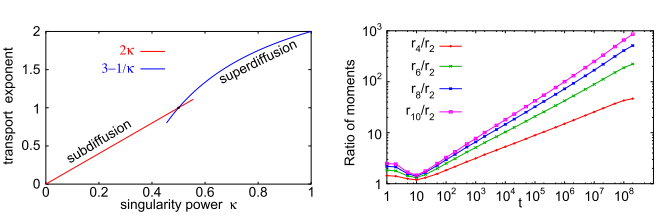

Fig. 7. (*Left*) Exponents of anomalous transport for power-law singularities of return time: transition from sub- to superdiffusion. (*Right*) Temporal evolution of ratios $r_n(t) = \langle (x(t) - \langle x(t) \rangle)^n \rangle^{1/n}$ of central moments for superdiffusive transport in the special flow with singularity $T(x) \sim |x - x_0|^{-2/3}$.

by equidistant distribution predicts $\xi^2(t) \sim \log^2 t$ for the asymmetric logarithmic singularity and, respectively, $\xi^2(t) \sim t^{2\kappa}$ for power-law singularities with $0 < \kappa < 1/2$. Both estimates are excellently matched by direct numerical simulations (compare Figs. 5 and 6).

Singularities in the range $1/2 \le \kappa < 1$ are too strong for the approach based on the equidistant distribution. Instead, we consider special flows over the random circle map: On reaching $T(u)$, the point jumps to the position, randomly chosen from the uniform distribution on the unit interval. Treating this process as a unidirectional continuous-time random walk (CTRW), we calculated the leading terms in the distribution of the number of jumps within the fixed time t. For the marginal (but relevant) case $\kappa = 1/2$ this yields the estimate

$$\xi^2(t) = \frac{\sqrt{2}}{16}\, t\, \log t - \frac{5 + \log 2}{16\sqrt{2}}\, t + \dots$$

which well matches the numerical results.

For $\kappa > 1/2$ the CRTW approach predicts superdiffusion with the leading term in the evolution of $\xi^2(t)$ proportional to $t^{3-1/\kappa}$; like the previous ones, this prediction was corroborated by comparison with numerics. Transition from subdiffusion with transport exponent 2κ to superdiffusion with transport exponent $3 - 1/\kappa$ is shown in Fig. 7.

Remarkably, transport in these special flows is not only superdiffusive but also multifractal. According to the CTRW calculation of the higher-order central moments

$$m_n(t) = \langle (x(t) - \langle x(t) \rangle)^n \rangle,$$

the dominating term for $1/2 < \kappa < 1/$ is given by $m_n(t) \sim t^{n+1-1/\kappa}$. In Fig. 7, *Right* we demonstrate the effect of multifractality for the case of the special flow with $\kappa = 2/3$ by comparing the values of $r_n(t) = \left(m_n(t)\right)^{1/n}$.

Conclusions

Summarizing, we have considered transport of tracers in plane steady viscous flows in a wide interval of temporal and spatial scales. In a contradistinction to chaotic turbulent flows that typically feature normal transport, the laminar plane steady viscous flows through periodic arrays of liquid or solid obstacles can display transport anomalies. This kind of anomalous transport is of purely deterministic origin: It is caused solely by divergence of the passage times near the obstacle. Depending on the geometry of the flow pattern, advection of passive tracers can be subdiffusive or superdiffusive. For the effect to take place, it is sufficient to have just one vortex or obstacle in every cell of the periodic flow pattern; if several singularities of passage time are present, the strongest of them determines the kind of transport anomaly. Otherwise, the effect is largely independent from the details of forcing or the injected energy. (Of course, the energy supplied by the forcing should suffice for the onset of vortices.) By using the construction of special flow over the circle map with appropriate singularities of passage time, we arrived at explicit estimates for the transport characteristics that well match the results of extensive numerical simulations. Although the present study is restricted to infinite periodic lattices of vortices or obstacles, qualitative predictions of this theory can be relevant also for spatially disordered flow patterns with appropriate types of passage time singularities.

ACKNOWLEDGMENTS. This research was supported by Grant I-1271-303.7/2014 from the German–Israeli Foundation for Scientific Research and Development.

1. Taylor GI (1953) Dispersion of soluble matter in the solvent flowing slowly through a tube. *Proc R Soc A* 219:186–203.
2. Shraiman BI (1987) Diffusive transport in a Rayleigh-Bénard convection cell. *Phys Rev A* 36:261–267.
3. Avellaneda M, Majda AJ (1990) Mathematical models with exact renormalization for turbulent transport. *Commun Math Phys* 138:381–429.
4. Solomon TH, Gollub JP (1988) Passive transport in steady Rayleigh-Bénard convection. *Phys Fluids* 31:1372–1379.
5. Solomon TH, Gollub JP (1988) Chaotic particle transport in time-dependent Rayleigh-Bénard convection. *Phys Rev A* 38:6280–6286.
6. Abarzhi SI, Gauthier S, Sreenivasan KR (2013) Turbulent mixing and beyond: Non-equilibrium processes from atomistic to astrophysical scales II. *Philos Trans A Math Phys Eng Sci* 371:20130268.
7. Stanic M, Stellingwerf RF, Cassibry JT, Abarzhi SI (2012) Scale coupling in Richtmyer-Meshkov flows induced by strong shocks. *Phys Plasmas* 19: 082706.
8. Swisher NC, et al. (2015) Rayleigh-Taylor mixing in supernova experiments. *Phys Plasmas* 22:102707.
9. Gat O, Procaccia I, Zeitak R (1998) Anomalous scaling in passive scalar advection: Monte Carlo Lagrangian trajectories. *Phys Rev Lett* 80:5536–5539.
10. Abarzhi SI (2010) On fundamentals of Rayleigh-Taylor turbulent mixing. *Europhys Lett* 91:35001.
11. Zaslavsky GM, Stevens D, Weitzner H (1993) Self-similar transport in incomplete chaos. *Phys Rev E* 48:1683–1694.
12. Majda AJ, Kramer PR (1999) Simplified models for turbulent diffusion: Theory, numerical modelling, and physical phenomena. *Phys Rep* 314:238–574.
13. Zaks MA, Pikovsky AS, Kurths J (1996) Steady viscous flow with fractal power spectrum. *Phys Rev Lett* 77:4338–4341.
14. Zaks MA, Straube AV (2002) Steady Stokes flow with long-range correlations, fractal Fourier spectrum and anomalous transport. *Phys Rev Lett* 89:244101.
15. Zaks MA (2005) Anomalous transport in steady plane flows of viscous fluids. *Chaotic Dynamics and Transport in Classical and Quantum Systems*, eds Collet P, et al. (Kluwer Academic, Dordrecht, The Netherlands), pp 401–412.
16. von Neumann J (1932) Zur Operatorenmethode in der Klassischen Mechanik. *Ann Math* 33:587–642. German.
17. Cornfeld IP, Fomin SV, Sinai YG (1982) *Ergodic Theory* (Springer, New York).
18. Sommeria J (1986) Experimental study of the two-dimensional inverse energy cascade in a square box. *J Fluid Mech* 170:139–168.
19. Hasimoto H (1959) On the periodic fundamental solution of the Stokes equations and their application to viscous flow past a cubic array of spheres, *J Fluid Mech* 5:317–328.
20. Sangani AS, Yao C (1988) Transport processes in random arrays of cylinders. II. Viscous flow. *Phys Fluids* 31:2435–2444.
21. Pikovsky AS, Zaks MA, Feudel U, Kurths J (1995) Singular continuous spectra in dissipative dynamical systems, *Phys Rev E* 52:285–296.
22. Kolmogorov AN (1953) On dynamical systems with an integral invariant on a torus. *Dokl Akad Nauk SSSR Ser Mat* 93:763–766.
23. Kochergin AV (1976) Nondegenerate saddle-points and absence of mixing. *Math Notes* 19:453–468.
24. Sinai YaG, Khanin KM (1992) Mixing for some classes of special flows over rotations of the circle. *Funct Anal Appl* 26:155–169.
25. Kochergin AV (1975) On mixing in special flows over translation of intervals and in smooth flows on surfaces. *Math Sbornik* 96:471–502.